Hindawi
Mathematical Problems in Engineering
Volume 2019, Article ID 9846305, 13 pages
https://doi.org/10.1155/2019/9846305

Research Article

Active-Side Calculation Method for a Backhoe Hydraulic Excavator with Incomplete Digging Resistance in a Normal State

Zhigui Ren,[1,2] **Junli Wang**,[1,2] **Jin Chen**,[3] **Junfeng Zhang**,[1] **Jurong Liu**,[1] **Yang Liang**,[1] **and Haoran Sun**[1]

[1]*School of Mechanical Engineering, Shaanxi University of Technology, Hanzhong 723000, China*
[2]*Shaanxi Key Laboratory of Industrial Automation, Shaanxi University of Technology, Hanzhong 723000, China*
[3]*State Key Laboratory of Mechanic Transmission, Chongqing University, Chongqing 400030, China*

Correspondence should be addressed to Zhigui Ren; ren_411@163.com

Received 18 January 2019; Revised 17 June 2019; Accepted 11 July 2019; Published 14 August 2019

Academic Editor: Mohammad Uddin

The digging resistance in a normal state is the key to excavator design and automated excavation. It is difficult to accurately predict, simulate, or directly measure the digging resistance in a normal state due to uncertainties in the soil properties and excavation parameters. In this paper, a research idea is proposed that uses the working device as the entry point to indirectly calculate the digging resistance in a normal state by measuring the motion parameters and the cylinder pressure intensity. Based on the rule of combination for spatial force systems, a method for combining and projecting the system of the digging resistance is proposed in which the system is projected as six parts, and the tangential force, normal force, and bending moment in the plane of symmetry of the working device are the objects of the solution to avoid redundant equations. Based on kinematics and dynamics models of the excavator and the force and moment equilibrium conditions of the working device, equations for the active-side calculation of the incomplete digging resistance are derived. Based on these equations, the motion parameters of the working device and data on the cylinder pressure intensity obtained by measurement are used to calculate the incomplete digging resistance. The validation scheme and process proposed use the incomplete digging resistance as the external load to obtain the simulated stress of the working device through transient analysis. The simulated stress and the measured stress corresponding to the position of the measurement point are extracted and compared. The results show that there is a difference in the size of the numerical value between the simulated and measured stress, but the variation law is highly consistent, which validates the calculation method. In this paper, an active-side calculation method is provided for the incomplete digging resistance in a normal state without considering the soil-tool interaction relationships, which lays a theoretical foundation for the study of the digging resistance characteristics in a normal state, as well as excavator design and automated excavation.

1. Introduction

In earthwork operations, the digging resistance is not only used in the design of an excavator and its working device but also the premise of automated excavation [1]. The studies about the digging resistance mainly focus on early soil-tool interaction relationships and the current digging resistance simulation modelling.

Based on the assumptions that the soil is homogeneous, continuous, and isotropic and that the bucket has a simple shape and moves stably, many scholars have proposed soil-tool interaction models, especially the equations for expressing the tangential force of the digging resistance and the empirical formulas for the digging resistance that are more broadly applied in terms of excavator design and automation. Using the soil-tool interaction model, some scholars have predicted and assessed the digging or traction force required in the excavation of extraterrestrial rock strata [2, 3], and some scholars have also analysed and compared the cutting forces predicted by different models [4, 5]. The results show that under the same conditions of soil parameters and digging parameters, there are great differences in the digging resistance results calculated based on different models [5].

With the development of numerical simulation technology, to more accurately predict the digging resistance, the discrete element model has become a research hotspot in connection with soil that has different properties (cohesionless, cohesion, and adhesion) [6–11]. Coetzee and Els [6] established a two-dimensional simulation model for the digging process of cohesionless granular materials, and the results show that the discrete element method is more accurate in predicting the amount of soil loading and the area and location of soil deformation but has comparatively low accuracy in predicting the material failure surface, traction force, and traction energy. Obermayr et al. [7, 8] used a triaxial compression test to check parameters such as the internal friction angle of the soil. Considering the macromechanical characteristics of the soil and by setting up the cohesive forces between the granular elements, a prediction model for the traction force of cohesive soil was established on the basis of the prediction model for the traction force of cohesionless soil. Through this model, the effects of the cutting depth and width on the traction force were predicted, and the traction force of cohesive soil was found to be three times that of cohesionless soil.

Furthermore, based on the study of diggability and excavator system identification, many scholars have carried out research work related to automatic digging [12–16]. Tafazoli et al. [12] developed a novel approach for experimental determination of the link parameters and friction coefficients. This method is beneficial to indirect measurement of the external forces and compensation for the link weights in teleoperated excavator. Hall and Daneshmend [13] summarized some practical techniques for reliability analysis and reviewed the maintenance data requirements, sources, and issues. Tafazoli et al. [14], Saeedi et al. [15], and Marshall et al. [16] have researched on the teleoperated excavator and autonomous excavator.

In summary, existing research methods have established soil-tool interaction models and simulation models for predicting the digging resistance based on idealised assumptions about the soil characteristics and modes of operation. However, there are great complexities and uncertainties in general excavation work, both in the soil characteristics and modes of operation. We refer to the general excavation actions of an excavator at a construction site (nonideal state) as excavation in a normal state. Research on the digging resistance in a normal state is the key to excavator design and automated excavation. However, the soil characteristics and modes of operation in a normal state of excavation are generally variable and difficult to predict, causing the digging resistance in a normal state to be difficult to accurately predict, simulate, or directly measure.

The working device, as the side that exerts the digging action in the digging process, is referred to as the active side, and the soil, as the side that is passively deformed and displaced, is referred to as the passive side. In this paper, a research idea is provided that uses the working device as the entry point to indirectly calculate the digging resistance by measuring the motion parameters of the working device and the cylinder pressure intensity. First, a method for combining and projecting the system of the digging resistance is proposed, and then on the basis of kinematics and dynamics models of the excavator, a method is proposed that uses the measurement data of the working device to calculate the incomplete digging resistance, which no longer relies on the complex tool-soil interaction model. Moreover, the bending moment is considered in this method, which avoids the problem of redundant equations in solving for the digging resistance. Finally, the idea of consistency in the variation law of the stress is used to validate this method through experiments on excavation in a normal state.

2. Combining and Projecting the System of the Digging Resistance

Due to the nonuniformity of the soil, in addition to the positive load, the digging resistance also includes the offset load and the lateral force. In general situations, however, the offset load and the lateral force are relatively small, and due to the bilateral symmetry of the working device, most scholars have simplified the digging resistance as a planar force system in the bilateral symmetry plane of the working device; that is, only the action of the positive load is considered.

As shown in Figure 1(a), Hemami et al. [17] divided the digging resistance into six parts. In the figure, f_1 to f_6 correspond to the force to compensate for the weight of the loaded soil, the compacting resistance of unloaded soil, the friction forces, the cutting resistance, the inertial force (for the loaded soil), and the force to move the empty bucket. This method classifies the complex system of the digging resistance into six forces with different properties; although it helps to reveal the soil-tool interaction mechanism, the magnitude of the force is difficult to quantify. The digging resistance model with a flat, wedge edge is used as a reference. Chen et al. [18] simplified the system of the digging resistance acting on the bucket-shaped device as the tangential force and normal force acting on the tips of the bucket teeth (Figure 1(b)) and proposed a method for measuring and calculating the digging resistance based on this. The specific calculation process is to arbitrarily select two equations from the three moment equilibrium equations of the working device and solve for the two unknown numbers, the tangential force and normal force, which leads to the problem of redundant equations. The results indicate that there are great differences in the tangential force and normal force obtained from different equations.

To solve the above problem, it is necessary to return to the real state of bucket excavation. In the process of excavation in a normal state, the bucket and the soil are in direct contact and interact. The inner and outer contact surfaces of the bucket are subjected to the force of friction and the force of extrusion, and the bucket teeth and cutting edge are subjected to the crushing resistance generated by soil fault and flow. The soil resistance experienced by the entire bucket constitutes a complex spatial force system that changes over time, which is referred to as the system of the digging resistance. Based on the rule of combination of force systems, an arbitrary force system in space can be combined at any point to become a resultant force and a resultant force-couple, and it

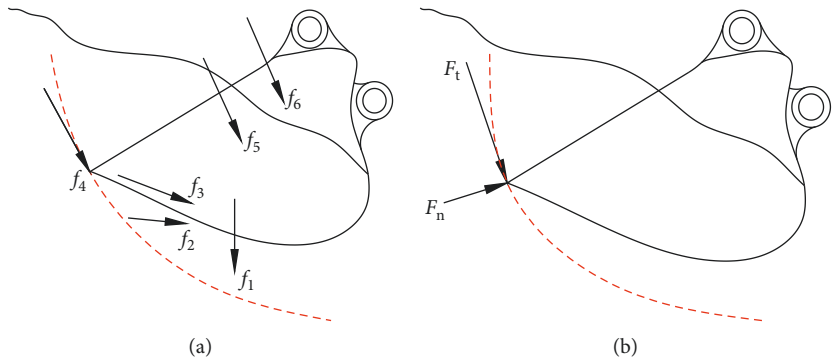

Figure 1: Existing method for simplifying the digging resistance.

can also be projected onto an arbitrary Cartesian coordinate system.

The cutting edge is one of the key parts for withstanding the action of soil obstruction. To facilitate research, the J-point (the midpoint of the cutting edge) is the point of synthesis for the system of the digging resistance (the origin of the coordinate system), and the motion trajectory of the J-point is referred to as the digging trajectory. The plane on which the digging trajectory is located (assuming there is no rotational motion in the digging process), that is, the bilateral symmetry plane of the working device, is a projection surface for the system of the digging resistance. On this projection surface, the tangential direction and normal direction of the digging trajectory are used as the X-axis and Y-axis of the Cartesian coordinate system, and the Z-axis is determined according to the right-hand rule. As shown in Figure 2(a), the projected coordinate system JXYZ of the digging resistance is established. The system of the digging resistance is combined at the J-point to become a resultant force and a resultant force-couple, and it is projected onto the X, Y, and Z axes. In accordance with the direction of action, the projections of the resultant forces on the X, Y, and Z axes are referred to as the tangential force F_t, normal force F_n, and lateral force F_l, respectively; in accordance with the characteristics of the action, the projections of the resultant force-couples on the X, Y, and Z axes are referred to as the torque moment M_t, rotational moment M_r, and bending moment M_b, respectively.

Due to the uncertainties in the object of digging and the mode of digging, it is almost impossible to achieve the direct solution of the resultant forces and the resultant force-couples. A method that can be tried is solving for their projections on the coordinate axes, that is, solving for the six components in Figure 2(a). However, it is not easy to simultaneously solve for these six components. Therefore, in this paper, the three unknown quantities for the system of the digging resistance projected onto the working device's plane of symmetry are solved first, that is, the tangential force F_t, normal force F_n, and bending moment M_b, as shown in Figure 2(b). In this paper, these three components are referred to as the incomplete digging resistance. The process for solving the incomplete digging resistance not only avoids the complexity of the system of the digging resistance but also avoids the problem of redundant equations caused by simplification.

3. Active-Side Calculation Method for the Incomplete Digging Resistance in a Normal State

A hydraulic excavator has multiple degrees of freedom. There are many compound actions in the digging process of a normal state. To determine the pose and coordinates of each component, a kinematics model needs to be established. The digging process is a dynamic process. To solve for the digging resistance, a dynamics model needs to be established first, and then the model for solving the digging resistance is finally obtained through force analysis.

3.1. Kinematics Model. The D-H coordinates system of the hydraulic excavator is established (Figure 3) [19, 20]. The relationship between adjacent coordinates systems ($o_i x_i y_i z_i$ and $o_j x_j y_j z_j$) can be expressed by the following four parameters: offset distance s_j (the distance from axis x_i to axis x_j along axis z_i), angle θ_j (the angle from axis x_i to axis x_j along axis z_i), rod length h_j (the distance from axis z_i to axis z_j along axis x_j), and torsion angle α_j (the angle from axis z_i to axis z_j along axis x_j). Also, s_j is set positive when coincident with the positive direction of axis z_i; θ_j is set positive when counterclockwise; h_j is set positive when in coincident with the positive direction of axis x_j; and α_j is set positive in the counterclockwise direction.

According to the establishment principle of the D-H coordinate system, S_0 is the distance from the boom with mounting hinge point A to the height of the shutdown surface, and $S_1 = S_2 = S_3 = 0$. h_0 is the distance from the boom with mounting hinge point A to the rotational axis Z_0 of the main engine, and h_1, h_2, and h_3 are the lengths of the boom AB, the arm BQ, and the bucket QJ, respectively. $\alpha_0 = \pi/2$, and $\alpha_1 = \alpha_2 = \alpha_3 = 0$. Let the coordinates of any point p in space under the i-th coordinate system be $[r_i] = [x_i, y_i, z_i]^T$ and the coordinates under the j-th coordinate system be $[r_j] = [x_j, y_j, z_j]^T$.

Set ${}^i r_p = \begin{bmatrix} r_i \\ 1 \end{bmatrix}$ and ${}^j r_p = \begin{bmatrix} r_j \\ 1 \end{bmatrix}$; then,

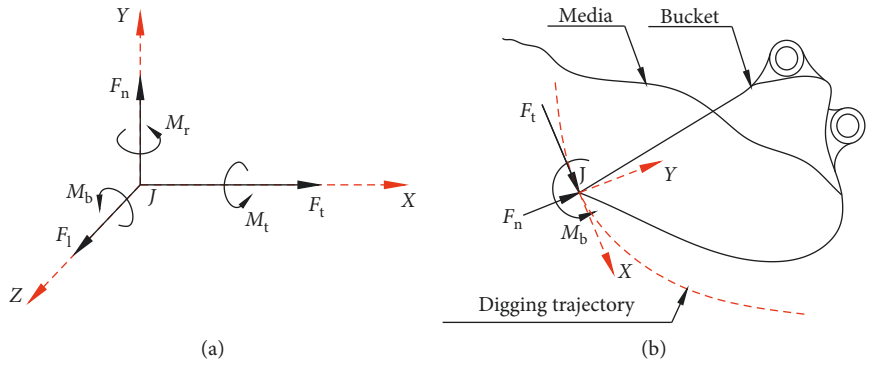

Figure 2: Combination and projection for the system of digging resistance.

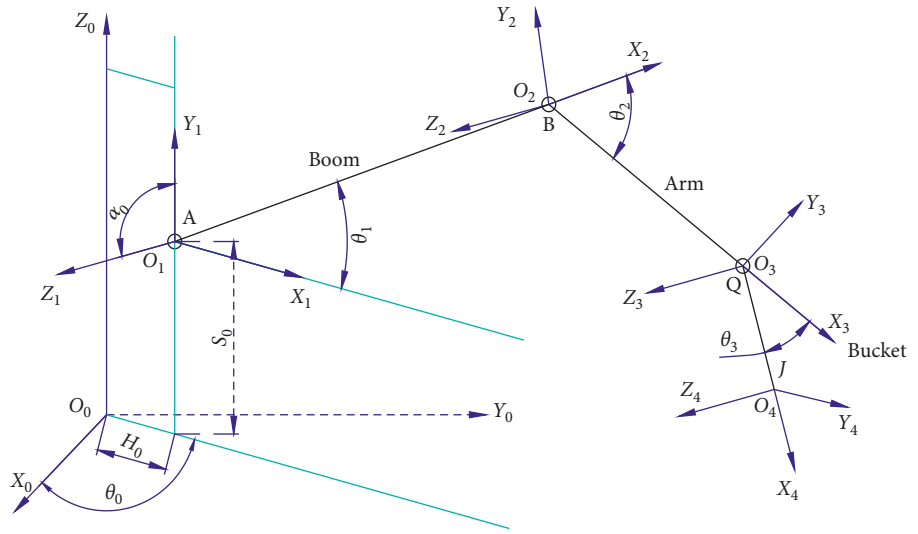

Figure 3: The D-H coordinate system of the hydraulic excavator.

$$\begin{cases} {}^{j}r_p = [M_{ij}]\,{}^{j}r_p, \\ {}^{j}r_p = [M_{ji}]\,{}^{j}r_p, \end{cases} \tag{1}$$

where $[M_{ij}]$ and $[M_{ij}]$ are, respectively, the transformation matrices between adjacent coordinate systems $o_j x_j y_j z_j$ and $o_i x_i y_i z_i$.

$$\begin{cases} [M_{ij}] = \begin{bmatrix} \cos\theta_i & -\sin\theta_i\cos\alpha_i & \sin\theta_i\sin\alpha_i & h_i\cos\theta_i \\ \sin\theta_i & \cos\theta_i\cos\alpha_i & -\cos\theta_i\sin\alpha_i & h_i\sin\theta_i \\ 0 & \sin\alpha_i & \cos\alpha_i & S_i \\ 0 & 0 & 0 & 1 \end{bmatrix}, \\ [M_{ji}] = \begin{bmatrix} \cos\theta_i & \sin\theta_i & 0 & -h_i \\ -\sin\theta_i\cos\alpha_i & \cos\theta_i\cos\alpha_i & \sin\alpha_i & -S_i \\ \sin\theta_i\sin\alpha_i & -\cos\theta_i\sin\alpha_i & \cos\alpha_i & 0 \\ 0 & 0 & 0 & 1 \end{bmatrix}. \end{cases} \tag{2}$$

3.2. Dynamics Model. The general form of the dynamics equation for the Lagrangian system is [12, 14]

$$T_i = \frac{d}{dt}\frac{\partial L}{\partial \dot{q}_i} - \frac{\partial L}{\partial q_i}, \quad i = 1, 2, \ldots, n, \tag{3}$$

where $L = K - P$ is referred to as the Lagrangian function, where K represents the kinetic energy of the system and P represents the potential energy of the system; T_i is the force or moment acting on the i-th coordinate system; n is the number of generalised links; q represents the generalised coordinates; and $\dot{q}$ represents the generalised velocity. For the excavator, T_i is the moment acting on the coordinate system O_i, $n = 4$, the boom, arm, and bucket are, respectively, the second, third, and fourth generalised links, and q and $\dot{q}$ correspond to θ and $\dot{\theta}$, respectively.

Let p be any one point on the generalised link i. According to formula (1),

$${}^{0}r_p = H_i\,{}^{i}r_p, \tag{4}$$

where H_i represents the transformation matrix from the local coordinate system O_i to the basic coordinate system O_0: $H_i = [M_{01}][M_{12}]\cdots[M_{(i-1)i}]$.

The velocity of the P-point is

$$ {}^0V_p = \frac{d}{d_t}\left({}^0r_p\right) = \dot{H}_i\, {}^i r_p = \left(\sum_{j=1}^{i}\frac{\partial H_i}{\partial \theta_j}\dot{\theta}_j\right){}^i r_p = \left(\sum_{j=1}^{i} U_{ij}\dot{\theta}_j\right){}^i r_p. \tag{5} $$

The square of the velocity of the P-point is

$$ \begin{aligned} \left({}^0V_p\right)^2 &= \left({}^0V_p\right)\cdot\left({}^0V_p\right) = \mathrm{Trace}\left[\left({}^0V_p\right)\cdot\left({}^0V_p\right)^T\right] \\ &= \mathrm{Trace}\left[\sum_{j=1}^{i}\sum_{k=1}^{i} U_{ij}\, {}^i r_p \left({}^i r_p\right)^T \left(U_{ik}\right)^T \dot{\theta}_j\dot{\theta}_k\right]. \end{aligned} \tag{6} $$

Set d_m as the mass of the P-point; then, its kinetic energy is

$$ \begin{aligned} dk_i &= \frac{1}{2}\left({}^0V_p\right)^2 d_m \\ &= \frac{1}{2}\mathrm{Trace}\left[\sum_{j=1}^{i}\sum_{k=1}^{i} U_{ij}\, {}^i r_p \left({}^i r_p\right)^T d_m \left(U_{ik}\right)^T \dot{\theta}_j\dot{\theta}_k\right]. \end{aligned} \tag{7} $$

Integrate the above equation over link i to obtain the kinetic energy of link i:

$$ K_i = \int_{\mathrm{Link}\, i} dk_i = \frac{1}{2}\mathrm{Trace}\left[\sum_{j=1}^{i}\sum_{k=1}^{i} U_{ij} I_i \left(U_{ik}\right)^T \dot{\theta}_j\dot{\theta}_k\right], \tag{8} $$

where $I_i = \int_{\mathrm{Link}\, i} {}^i r_p \cdot \left({}^i r_p\right)^T \cdot d_m$ is the pseudoinertial matrix of link i. In formulas (5) to (8), U_{ij} and U_{ik} represent the derivations of the i-th and j-th generalised coordinates by the transformation matrix H_i, respectively.

The kinetic energy of the driving device of the link i is

$$ K_{ai} = \frac{1}{2} I_{ai}\dot{\theta}_i^2. \tag{9} $$

The total kinetic energy of the excavator system is obtained in accordance with formulas (8) to (9):

$$ K = \frac{1}{2}\sum_{i=1}^{4}\sum_{j=1}^{i}\sum_{k=1}^{i}\mathrm{Trace}\left(U_{ij} I_i \left(U_{ik}\right)^T\right)\dot{\theta}_j\dot{\theta}_k + \frac{1}{2}\sum_{i=1}^{4} I_{ai}\dot{\theta}_i^2. \tag{10} $$

The total potential energy of the excavator system is

$$ P = -\sum_{i=1}^{4} m_i g^T \left({}^0T_i \overline{r}_i\right). \tag{11} $$

Substitute formulas (10) and (11) into formula (3) to obtain the dynamics equation of the hydraulic excavator system:

$$ T_i = \sum_{j=1}^{4} D_{ij}\ddot{\theta}_j + I_{aj} q\ddot{\theta} + \sum_{j=1}^{4}\sum_{k=1}^{4} D_{ijk}\dot{\theta}_j\dot{\theta}_k + D_i, \quad i = 1, 2, 3, 4, \tag{12} $$

where $D_{ij} = \sum_{p=\max(i,j)}^{n}\mathrm{Trace}\left(U_{pj} I_p U_{pi}^T\right)$, $D_{ijk} = \sum_{p=\max(i,j,k)}^{n}\mathrm{Trace}\left(U_{pjk} I_p U_{pi}^T\right)$, and $D_i = \sum_{p=i}^{n} - m_p g^T U_{pi}\, {}^p r_p$, where U_{pjk} represents the second-order derivative of the transformation matrix H_p with regard to the two generalised j-th and k-th coordinates.

3.3. Calculation Model for the Incomplete Digging Resistance in a Normal State. As described above, T_i in formula (12) is the moment acting on coordinate system O_i. To establish the digging resistance model, it is first necessary to perform a force analysis to obtain the resultant moments acting on each coordinate system of the excavator's working device.

According to the combination result of the system of the digging resistance at the symmetry centre J-point of the cutting edge in the second section, with the exception of having power, the force situation in the symmetry plane of the hydraulic excavator's working device is as shown in Figure 4. F_{bo}, F_a, and F_{bu} represent the thrusts of the hydraulic cylinder of the boom, the hydraulic cylinder of the arm, and the hydraulic cylinder of the bucket, respectively, and F_{KL} represents the force of the link KL acting on the hinge point L. There is a definite relationship between F_{KL} and F_{bu}, that is, $F_{KL} = f(F_{bu})$. The resultant moments acting on the coordinate system of the boom O_2, the coordinate system of the arm O_3, and the coordinate system of the bucket O_4 are

$$ \begin{cases} T_2 = \overrightarrow{AC}\times\overrightarrow{F_{bo}} + \overrightarrow{AJ}\times\overrightarrow{F_t} + \overrightarrow{AJ}\times\overrightarrow{F_n} + M_b, \\ T_3 = \overrightarrow{BH}\times\overrightarrow{F_a} + \overrightarrow{BJ}\times\overrightarrow{F_t} + \overrightarrow{BJ}\times\overrightarrow{F_n} + M_b, \\ T_4 = \overrightarrow{QL}\times\overrightarrow{F_{KL}} + \overrightarrow{QJ}\times\overrightarrow{F_t} + \overrightarrow{QJ}\times\overrightarrow{F_n} + M_b. \end{cases} \tag{13} $$

The simultaneous use of formulas (12) and (13) results in moment equilibrium formula (14) containing the three components of the digging resistance. The incomplete digging resistance can be obtained by solving for these equations, but all six components for the system of the digging resistance cannot be completely obtained; therefore, these equations are referred to as the calculation model for the incomplete digging resistance in a normal state:

$$ \begin{aligned} &\overrightarrow{AC}\times\overrightarrow{F_{bo}} + \overrightarrow{AJ}\times\overrightarrow{F_t} + \overrightarrow{AJ}\times\overrightarrow{F_n} + M_b \\ &\quad = \sum_{j=1}^{4} D_{2j}\ddot{\theta}_j + I_{aj}\ddot{\theta}_2 + \sum_{j=1}^{4}\sum_{k=1}^{4} D_{2jk}\dot{\theta}_j\dot{\theta}_k + D_2, \\ &\overrightarrow{BH}\times\overrightarrow{F_a} + \overrightarrow{BJ}\times\overrightarrow{F_t} + \overrightarrow{BJ}\times\overrightarrow{F_n} + M_b \\ &\quad = \sum_{j=1}^{4} D_{3j}\ddot{\theta}_j + I_{aj}\ddot{\theta}_3 + \sum_{j=1}^{4}\sum_{k=1}^{4} D_{3jk}\dot{\theta}_j\dot{\theta}_k + D_3, \\ &\overrightarrow{QL}\times\overrightarrow{F_{KL}} + \overrightarrow{QJ}\times\overrightarrow{F_t} + \overrightarrow{QJ}\times\overrightarrow{F_n} + M_b \\ &\quad = \sum_{j=1}^{4} D_{4j}\ddot{\theta}_j + I_{aj}\ddot{\theta}_4 + \sum_{j=1}^{4}\sum_{k=1}^{4} D_{4jk}\dot{\theta}_j\dot{\theta}_k + D_4. \end{aligned} \tag{14} $$

For a given excavator, the geometric size and mass distribution are known. Using the kinematics and dynamics models of the excavator established in the previous text, the functions for the relative angle θ, angular velocity $\dot{\theta}$, and angular acceleration $\ddot{\theta}$ between various coordinate systems are given on the right side of the equations in formula (14). Therefore, if these motion parameters are measured, then the right part of the equations can be determined. At the same time, if the relative angle θ between various coordinate systems is measured, in accordance with the kinematics

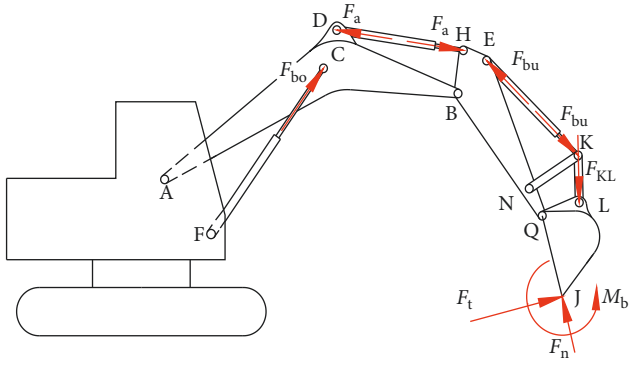

Figure 4: Force analysis in the symmetry plane of the excavator's working device.

model of the excavator, the direction of each acting force on the left side of the equations in formula (14) as well as the moment arm vectors corresponding to various acting forces can also be determined. If data on the cylinder pressure intensity are collected, then the thrusts applied to the working device by the hydraulic cylinders can be obtained, so F_{bo}, F_a, and F_{bu} can be determined. According to the force transfer mechanism, the thrust F_{KL} ($F_{KL} = f(F_{bu})$) transferred from the bucket's hydraulic cylinder to the link KL to ultimately act on the hinge point L can be calculated.

In summary, if the motion parameters of the components and the data on the cylinder pressure intensity can be measured, with the exception of the incomplete digging resistance, the other variables in formula (14) can all be determined. The incomplete digging resistance variables F_t, F_n, and M_b can be obtained by solving formula (14). In this method, there is no need to take into account the soil characteristics, bucket shape, and digging parameters, and there is also no need to take into account the soil-tool interaction relationship; the incomplete digging resistance can be calculated by measuring the active-side motion parameters of the excavator's main engine and collecting data on the cylinder pressure intensity. We refer to this method as the active-side calculation method for the incomplete digging resistance in a normal state.

4. Experimental Validation

A validation scheme was designed for the active-side calculation method for the incomplete digging resistance in a normal state (Figure 5). First, the motion parameters of each component and the data on the cylinder pressure intensity collected were substituted into formula (14) to calculate the incomplete digging resistance. Then, each component load of the working device was calculated according to the force and moment equilibrium equations for the boom, arm, and bucket, using transient analysis to obtain the simulated stress for each component. Finally, the simulated stress and measured stress were compared. If they were consistent with each other, then the load applied for the simulation was correct. The correctness of the load then suggested that the incomplete digging resistance was correct, so the active-side calculation method for the incomplete digging resistance in a normal state could be validated in the reverse direction.

According to the validation scheme, it is necessary to measure the motion parameters of each component in the digging process in a normal state as well as collect data on the cylinder pressure intensity and working device stress.

4.1. Building a Measurement Platform

4.1.1. Angular Displacement Measurement. Three NS-RB type angular displacement sensors were used to separately measure the angular displacement θ of the boom relative to the frame, the arm relative to the boom, and the bucket relative to the arm. The rotation axis of the angular displacement sensor remained concentrically and firmly connected with the pin axis of the component being measured through the shaft coupling. The outer casing of the angular displacement sensor was firmly connected with the component being measured through the mounting rack.

4.1.2. Pressure Intensity Measurement. Six NS-F type pressure sensors (0~50 MPa) were used to separately acquire data on the pressure intensities of the rod cavity and rodless cavity for the hydraulic cylinders of the boom, bucket rod, and bucket. Their mounting positions were the reserved pressure measurement points of each drive hydraulic cylinder.

4.1.3. Stress Measurement. Right angle-45° type strain rosettes were used to separately measure the strain at measurement points in the 0°, 45°, and 90° directions. The approach used for bridging the strain rosettes was the 1/4 bridging method, and compensation lines were used to compensate for the conductor resistance. The dynamic stress was more obvious at the positions on the working device with greater stress as the load changed, and the correlation with the digging resistance was stronger. Selecting these positions as the measurement points could better validate the digging resistance. Eight dynamic stress measurement points were selected according to the form of failure for the excavator's working device and the general law of the stress distribution in combination with the need to adhere the patch of the strain gauge. The layout for some of the measurement points is as shown in Figure 6.

4.1.4. Data Acquisition System. A NS-DAC3000 multichannel data acquisition system was used to simultaneously acquire the feedback signals from three angular displacement sensors and six pressure sensors. A DRA-30A multichannel dynamic-static strain gauge was used to acquire the feedback data at the eight dynamic stress measurement points. The time interval of data acquisition was set to 10 milliseconds during the test.

The measurement object was a 36-t backhoe hydraulic excavator. The testing location was a certain proving ground in Huzhou, China. The excavation object was Class III soil mixed with small stones (the active-side calculation method

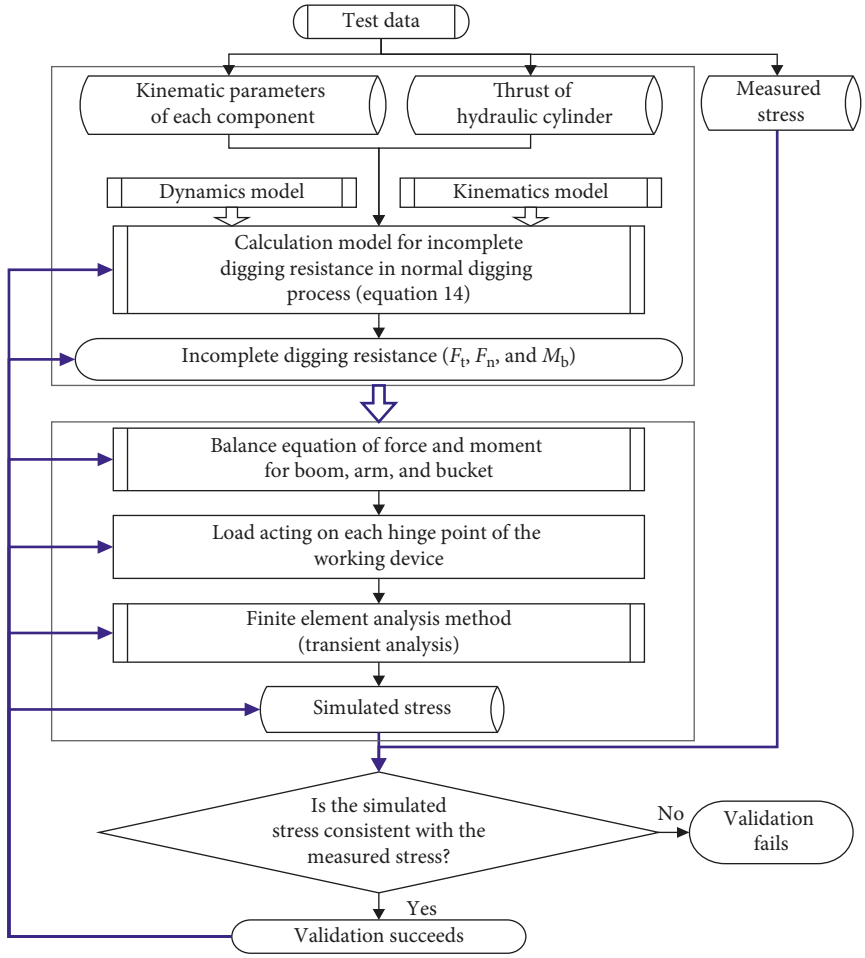

Figure 5: Validation scheme for the digging resistance-stress measurement.

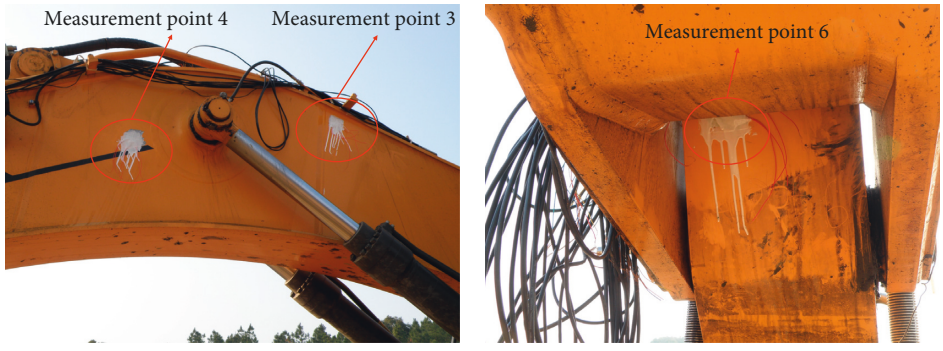

Figure 6: Layout of the stress measurement points.

for the digging resistance proposed in this paper was unrelated to the soil-tool interaction model; therefore, characteristics such as the soil density and viscosity were not of concern during the measurement process). A comprehensive measurement platform that includes angular displacement, pressure intensity, and stress measurements is shown in Figure 7.

4.2. Calculating the Incomplete Digging Resistance in a Normal State

4.2.1. Conversion of Measurement Data. The actual angles between the boom and the mounting, the arm and the boom, and the bucket and the arm were

$$\theta_i = \theta_{i\min} + \theta_{i\,\text{measurement}} - \theta'_{i\,\text{measurement}}, \quad i = 1, 2, 3, \tag{15}$$

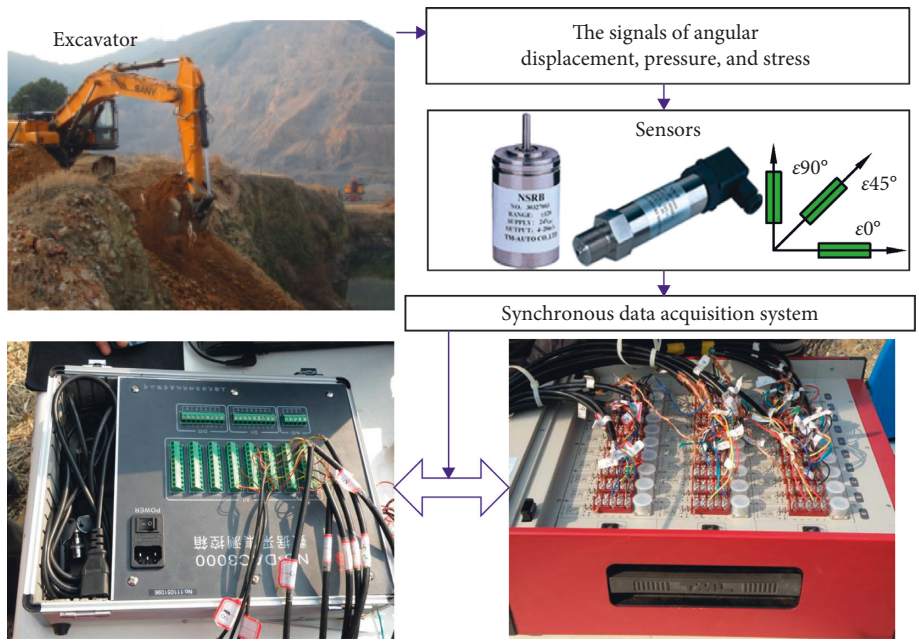

Figure 7: Comprehensive measurement platform.

where $\theta_{i\,\min}$ is the starting value (minimum value) of the joint space variable of the working device, while $\theta'_{i\,\text{measurement}}$ and $\theta_{i\,\text{measurement}}$ are, respectively, the initial value and real-time measurement value of the three angular displacement sensors.

The thrusts for the hydraulic cylinders of the boom, arm, and bucket were

$$\begin{cases} F_{\text{bo}} = \left(\dfrac{\pi D_{1a}^2}{4} P_{1a} - \dfrac{\pi\left(D_{1a}^2 - D_{1i}^2\right)}{4} P_{1i}\right) n_1, \\ F_{\text{a}} = \left(\dfrac{\pi D_{2a}^2}{4} P_{2a} - \dfrac{\pi\left(D_{2a}^2 - D_{2i}^2\right)}{4} P_{2i}\right) n_2, \\ F_{\text{bu}} = \left(\dfrac{\pi D_{3a}^2}{4} P_{3a} - \dfrac{\pi\left(D_{3a}^2 - D_{3i}^2\right)}{4} P_{3i}\right) n_3, \end{cases} \tag{16}$$

where p_{1i}, p_{1a}, p_{2i}, p_{2a}, p_{3i}, and p_{3a} are the measured pressure intensities of the rod cavity and rodless cavity for the hydraulic cylinders of the boom, arm, and bucket; D_{1i}, D_{1a}, D_{2i}, D_{2a}, D_{3i}, and D_{3a} are the diameter intensities of the rod cavity and rodless cavity for the hydraulic cylinders of the boom, arm, and bucket; and n_1, n_2, and n_3 are the number intensities of the hydraulic cylinders for the boom, arm, and bucket.

4.2.2. Fitting of Measurement Data and Calculation of Digging Resistance. To eliminate the effects of noise and impact in the measurement process, a fitting process was first carried out on the converted data for the angular displacement and cylinder thrust. The angular velocity ω was obtained by taking the derivative of the fitting function θ for the angular displacement data with respect to time, and the angular acceleration α was obtained by taking the derivative of the angular velocity ω with respect to time. The motion parameters (angular displacement θ, angular velocity ω, and angular acceleration α) of each component after fitting and the data on the hydraulic cylinder thrusts were substituted into formula (14) to calculate the tangential force F_{t}, normal force F_{n}, and bending moment M_{b}.

For this measurement, multiple instances of digging were completed under different working conditions. The digging process of working condition *I* selected in this paper illustrated the processing of the measurement data and the solution and validation of the digging resistance. Working condition *I* was a digging experiment in which a skilled operator fully loaded the bucket in a normal state according to the habitual manner of operation in the main operation area of the excavator. Figure 8 shows the raw data and fitting data of the angular displacement θ, the angular velocity ω, and the angular acceleration α, as well as the raw data and fitting data of the hydraulic cylinder thrusts corresponding to the digging process of working condition *I*. It can be seen from Figure 8 that there were great changes in the angular displacement of the bucket relative to the boom and the arm in this instance of the digging process. The angular velocity and angular acceleration showed continuous fluctuation, and the hydraulic cylinder of the boom was in a passive state of tension prior to 4 s and then started to actively extend outward to carry out the lifting action. Using the angular displacement data and the kinematics model of the excavator, the restored trajectory of the digging process was obtained (Figure 9). As shown in Figure 9, the boom, arm, and bucket have more linkage actions in the digging process, indicating that composite digging is a commonly used operation mode for digging in a normal state.

Figure 10 shows the calculation results for the incomplete digging resistance in the digging process of working condition *I*. *F* represents the resultant force for the

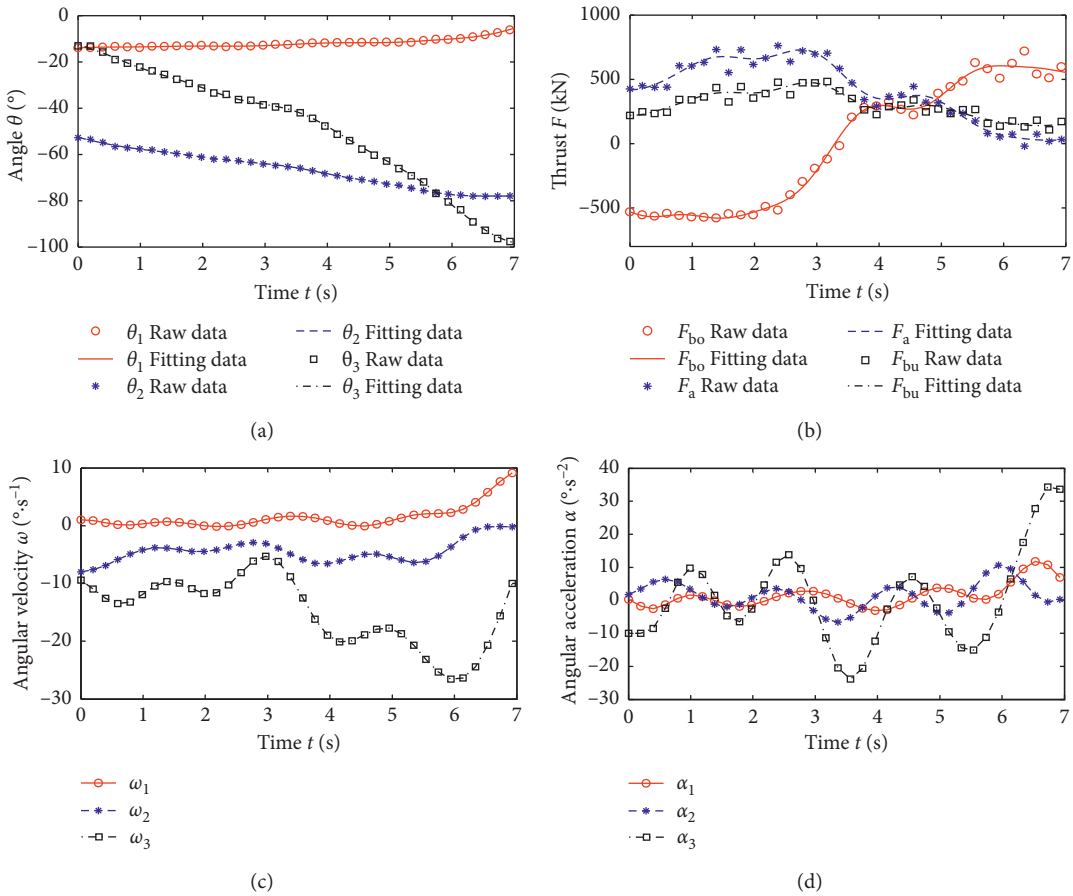

Figure 8: Data processing and fitting results.

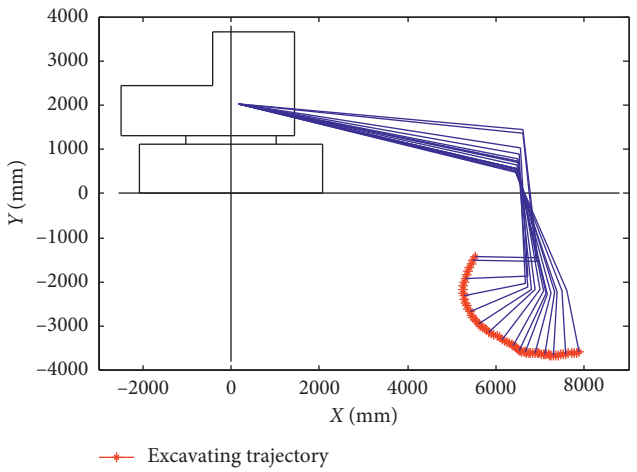

Figure 9: Restored trajectory of the digging process.

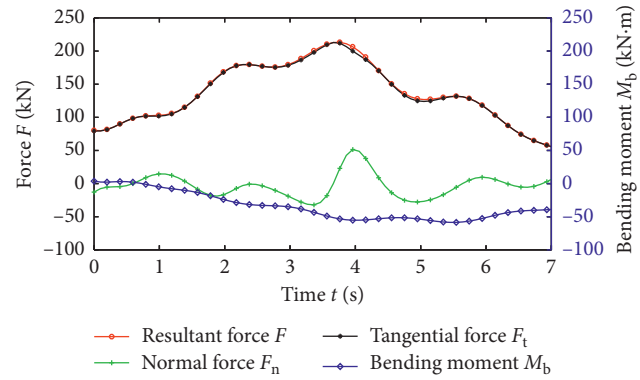

Figure 10: Calculated digging resistance.

system of digging resistance projected onto the symmetry plane of the working device, and $\overrightarrow{F} = \overrightarrow{F_t} + \overrightarrow{F_n}$. The results of Figure 10 indicate that the tangential force F_t is the main component of the resultant force F as the normal force is relatively small and its direction changes continuously with the digging process. The effect of the bending moment M_b is smaller than the moment effect from the tangential force on each hinge point. The acquisition of the incomplete digging resistance in a normal state lays the foundation for research on the characteristics of the digging resistance, which will help with checking the strength characteristics and optimising the structural design of excavators, as well as with research on automated excavation.

4.3. Calculating the Measured Stress and the Simulated Stress

4.3.1. Measured Stress. The three-direction strain rosette could acquire in real time the strains ε_x, ε_y, and $\varepsilon_{45°}$, which

corresponded to the measurement points in the directions of 0°, 90°, and 45°. The elastic modulus E and Poisson's ratio μ for the material at the measurement points of the working device were known. The maximum and minimum normal stresses at the measurement point were

$$\begin{cases} \sigma_1 = \dfrac{E\left(\varepsilon_x + \varepsilon_y\right)}{2\left(1-\mu\right)} + \dfrac{E}{2\left(1+\mu\right)}\sqrt{\left(\varepsilon_x - \varepsilon_y\right)^2 + \left(\varepsilon_x + \varepsilon_y - 2\varepsilon_{45^\circ}\right)^2}, \\ \sigma_3 = \dfrac{E\left(\varepsilon_x + \varepsilon_y\right)}{2\left(1-\mu\right)} - \dfrac{E}{2\left(1+\mu\right)}\sqrt{\left(\varepsilon_x - \varepsilon_y\right)^2 + \left(\varepsilon_x + \varepsilon_y - 2\varepsilon_{45^\circ}\right)^2}. \end{cases} \tag{17}$$

The equivalent stress of the measurement point was calculated according to the fourth strength theory:

$$\sigma_{r4} = \sqrt{\sigma_1^2 + \sigma_3^2 - \sigma_1 * \sigma_3}. \tag{18}$$

The curve for the change in stress in the digging process corresponding to the measurement point could be calculated by substituting the strain data obtained from the measurement into formulas (17) and (18).

4.3.2. Simulated Stress. When the bucket touches the soil and leaves the ground, the digging resistance will change obviously, which can determine whether the excavator is in the digging state. The trajectory in the digging state is selected as the object of simulation analysis.

Using the incomplete digging resistance and the thrusts of the various hydraulic cylinders obtained in Section 4.2, the force at each hinge point of the working device was calculated according to the force and moment equilibrium equations of the boom, arm, and bucket, that is, the dynamic load spectrum of each component in the operation process in a normal state.

A three-dimensional model of the boom and the arm was established in Creo. Hypermesh was used to carry out mesh generation on it and to define the material attributes and element attributes. The preprocessed model was introduced into Patran. The boom and arm were both regarded as cantilever structures, and corresponding constraints and loads were applied. The loads include the gravity load and the dynamic load on each hinge point that varied with time, and all loads needed to be converted to the corresponding coordinate system of the body. Afterwards, calculations for the simulation of the dynamic stress were carried out to obtain the variation law of the stress with time for the boom and arm under various digging working conditions.

5. Results and Discussion

5.1. Comparing the Simulated Stress with the Measured Stress. The stress spectrum at the location of each measurement point was extracted from the simulation results in Section 4.3.2 and compared with the measured stress. The stress comparison diagram of each measurement point on the boom and arm in the digging process of working condition *I* is shown in Figure 11.

Through the correlation of the values of the simulated stress and the measured stress in Figure 11 and each of the other working conditions, it can be seen that the variation laws for the simulated stress and the measured stress were highly consistent; the measured stress was generally larger than the simulated stress, with measurement point 3 and measurement point 5 showing the most obvious differences, close to 30% of the measured stress.

5.2. Discussion. Comparing the measurement process and the simulation process, there are several possible reasons for the above difference: (1) The actual system of the digging resistance in the measurement process was composed of six parts, but only the incomplete digging resistance solved in this paper was applied in the simulation model. The incomplete external load applied to the simulation process caused the simulated stress to be smaller than the measured stress. (2) There were influencing factors, such as welding seams and dead weight in the measurement prototype. These factors, which were not considered in the simulation process, caused the simulated stress to be smaller than the measured stress. (3) There was a certain deviation between the coordinate position of the stress extracted in the simulation model and the position of the actual measurement point, which caused a certain deviation in the simulated stress.

Measurement point 3 and measurement point 5 were symmetrically distributed at vertex positions of the box-shaped structure on both sides of the boom's bending beam. Because they were located on both sides of the box-shaped structure, they were most affected by the lateral force; at the same time, due to their proximity to the two welding seams at the position where the thickness of the steel plate changed, they were subjected to the greatest effect of the concentrated stress caused by the welding seams. The lateral force was not considered in the simulation process, and the concentrated stress caused by the welding seams was also not taken into account. These are the main reasons why the measured stresses at measurement point 3 and measurement point 5 were obviously larger than the simulated stresses.

In comparing the simulated stresses and measured stresses of the eight measurement points under all working conditions measured, the results were consistent with Figure 11: the simulated stress was highly consistent with the measured stress in terms of the variation law, but there were certain differences in the numerical values (the simulated stress was generally smaller than the measured stress). The high consistency between the simulated stress and measured stress in the variation law verifies the correctness of the calculation model (formula (14)) proposed in this paper, and the difference in the numerical value indicates that the completeness (accuracy) of the model needs to be improved.

As shown in the validated relationship in Figure 5, the high consistency in the variation law indicates the reliability of the calculation process for the simulated stress. The load is the premise of the simulation, and the reliability of the simulation process indicates the correctness of the load. The

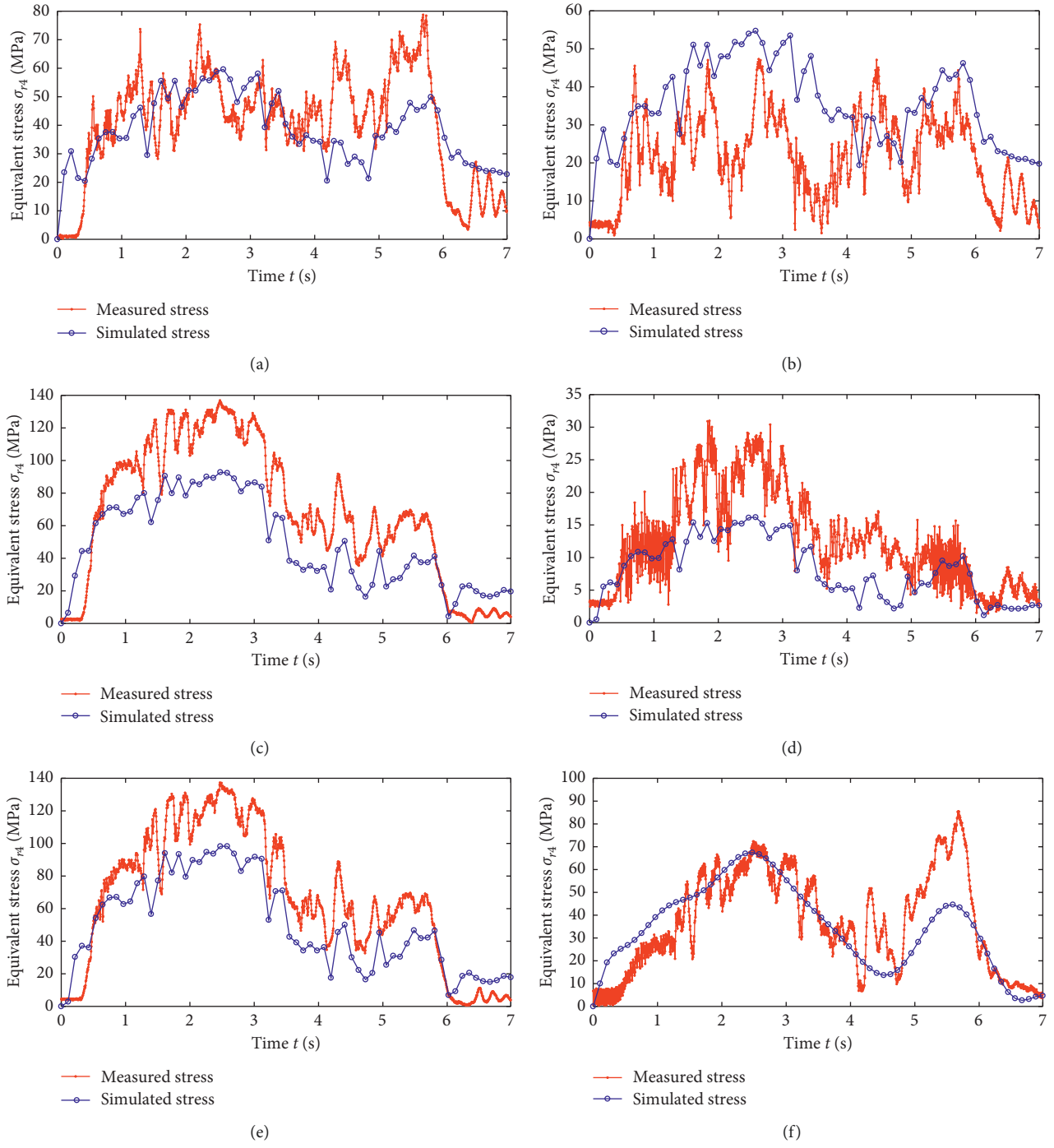

Figure 11: Continued.

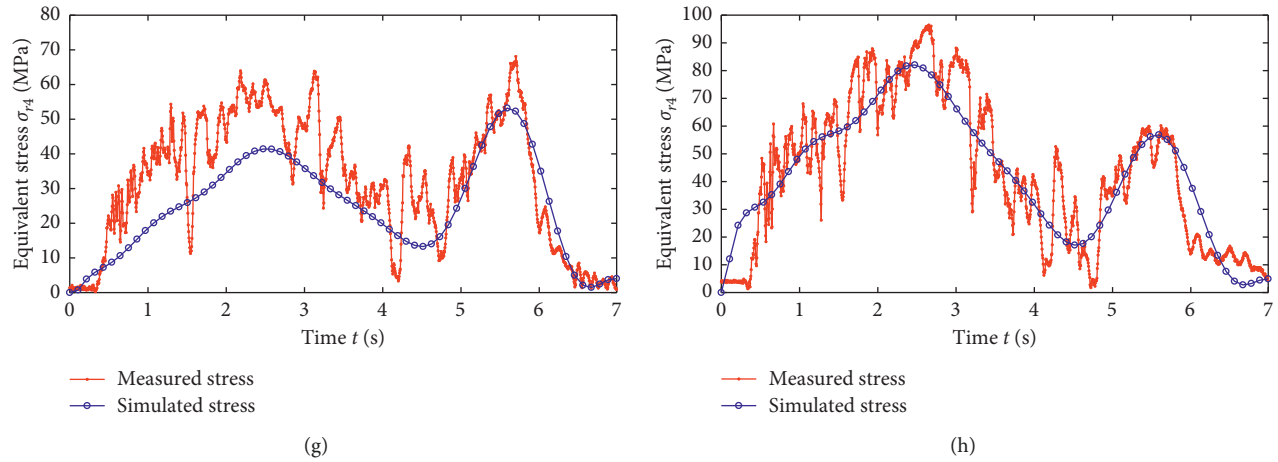

Figure 11: Comparison between simulated and measured stress. (a) Measurement point 1. (b) Measurement point 2. (c) Measurement point 3. (d) Measurement point 4. (e) Measurement point 5. (f) Measurement point 6. (g) Measurement point 7. (h) Measurement point 8.

load is obtained by solving for the incomplete digging resistance, and the correctness of the load indicates the correctness of the incomplete digging resistance and thereby the correctness of the active-side calculation method for the incomplete digging resistance in a normal state.

As described above, the main reason for this difference is that the active-side calculation method for the digging resistance in a normal state proposed in this paper could only obtain the incomplete digging resistance, and the remaining three components for the system of the digging resistance were not calculated; hence, there was no way for them to become loads to be applied to the simulation model. We speculated that if the remaining three parts of the system of the digging resistance could be calculated to make the simulated load closer to the actual load, the difference between the simulated stress and the measured stress would be further reduced.

6. Conclusion

To solve the problem of solving for the digging resistance in a normal state, the rule of combination for spatial force systems was used to propose a method for combining and projecting the system of the digging resistance, and the incomplete digging resistance became the target to be solved in this paper. An active-side calculation method for the incomplete digging resistance in a normal state was proposed based on kinematics and dynamics models of the excavator and the moment equilibrium equations of the working device. This method does not require consideration of the soil characteristics, bucket shape, or digging parameters; the incomplete digging resistance is instead calculated according to the motion parameters of the working device and data collected on the cylinder pressure intensity during the digging process in a normal state. This provides preconditions for research on the digging resistance in a normal state and lays a theoretical foundation for excavator design and automated excavation.

To validate the active-side calculation method for the incomplete digging resistance in a normal state, a scheme for measuring, calculating, and validating the digging resistance was proposed. Through the comprehensive measurement platform, the angular displacement and pressure intensity data needed to calculate the digging resistance and the stress data needed to validate the digging resistance were synchronously acquired. The calculated incomplete digging resistance in a normal state was used to calculate the load on each hinge point according to the force and moment equilibrium equations of the working device, and the simulated stresses of the boom and arm were obtained through the transient analysis method. In comparing the simulated stress extracted from the position corresponding to a measurement point with the measured stress, the results show that there is a difference in magnitude (the maximum value of the difference is close to 30% of the measured stress), but the variation laws are highly consistent.

The method for combining and projecting the system of the digging resistance and the calculation method for the incomplete digging resistance provide a theoretical foundation and have meaning as a reference for completely solving the six unknown quantities in the system of the digging resistance.

Data Availability

The data used to support the findings of this study have been deposited in the figshare repository (DOI: 10.6084/m9.figshare.7613093; persistent identifier: https://figshare.com/s/935ca15830608e7f8145).

Conflicts of Interest

The authors declare that there are no conflicts of interest regarding the publication of this paper.

Acknowledgments

This work was funded by the National Natural Science Foundation of China (no. 51605270), the Natural Science Research Project of Shaanxi Province (no. 2019JQ-884), the

Shaanxi Provincial Department of Education Scientific Research Project (no. 15JK1136), and the Research Project of Shaanxi University of Technology (no. SLGQD15-09).

References

[1] S. Blouin, A. Hemami, and M. Lipsett, "Review of resistive force models for earthmoving processes," *Journal of Aerospace Engineering*, vol. 14, no. 3, pp. 102–111, 2001.

[2] A. Wilkinson and A. DeGennaro, "Digging and pushing lunar regolith: classical soil mechanics and the forces needed for excavation and traction," *Journal of Terramechanics*, vol. 44, no. 2, pp. 133–152, 2007.

[3] L. Masafumi and G. Leslie, "Excavation of lunar regolith with large grains by rippers for improved excavation efficiency," *Journal of Aerospace Engineering*, vol. 26, no. 1, pp. 97–104, 2013.

[4] B. P. Patel and J. M. Prajapati, "Evaluation of resistive force using principle of soil mechanics for mini hydraulic backhoe excavator," *International Journal of Machine Learning and Computing*, vol. 2, no. 4, pp. 386–391, 2012.

[5] R. J. Godwin and M. J. O'Dogherty, "Integrated soil tillage force prediction models," *Journal of Terramechanics*, vol. 44, no. 1, pp. 3–14, 2007.

[6] C. J. Coetzee and D. N. J. Els, "The numerical modelling of excavator bucket filling using DEM," *Journal of Terramechanics*, vol. 46, no. 5, pp. 217–227, 2009.

[7] M. Obermayr, K. Dressler, C. Vrettos, and P. Eberhard, "Prediction of draft forces in cohesionless soil with the discrete element method," *Journal of Terramechanics*, vol. 48, no. 5, pp. 347–358, 2011.

[8] M. Obermayr, C. Vrettos, P. Eberhard, and T. Däuwel, "A discrete element model and its experimental validation for the prediction of draft forces in cohesive soil," *Journal of Terramechanics*, vol. 53, pp. 93–104, 2014.

[9] E. L. Bravo, E. Tijskens, M. H. Suárez, O. Gonzalez Cueto, and H. Ramon, "Prediction model for non-inversion soil tillage implemented on discrete element method," *Computers and Electronics in Agriculture*, vol. 106, pp. 120–127, 2014.

[10] M. Ucgul, J. M. Fielke, and C. Saunders, "Three-dimensional discrete element modelling (DEM) of tillage: accounting for soil cohesion and adhesion," *Biosystems Engineering*, vol. 129, pp. 298–306, 2015.

[11] B. Li, Y. Chen, and J. Chen, "Modeling of soil-claw interaction using the discrete element method (DEM)," *Soil and Tillage Research*, vol. 158, pp. 177–185, 2016.

[12] S. Tafazoli, P. D. Lawrence, and S. E. Salcudean, "Identification of inertial and friction parameters for excavator arms," *IEEE Transactions on Robotics and Automation*, vol. 15, no. 5, pp. 966–971, 1999.

[13] R. A. Hall and L. K. Daneshmend, "Reliability modelling of surface mining equipment: data gathering and analysis methodologies," *International Journal of Surface Mining, Reclamation and Environment*, vol. 17, no. 3, pp. 139–155, 2003.

[14] S. Tafazoli, S. E. Salcudean, K. Hashtrudi-Zaad, and P. D. Lawrence, "Impedance control of a teleoperated excavator," *IEEE Transactions on Control Systems Technology*, vol. 10, no. 3, pp. 355–367, 2002.

[15] P. Saeedi, P. D. Lawrence, D. G. Lowe et al., "An autonomous excavator with vision-based track-slippage control," *IEEE Transactions on Control Systems Technology*, vol. 13, no. 1, pp. 67–84, 2005.

[16] J. A. Marshall, P. F. Murphy, and L. K. Daneshmend, "Toward autonomous excavation of fragmented rock: full-scale experiments," *IEEE Transactions on Automation Science and Engineering*, vol. 5, no. 3, pp. 562–566, 2008.

[17] A. Hemami, S. Goulet, and M. Aubertin, "Resistance of particulate media to excavation: application to bucket loading," *International Journal of Surface Mining, Reclamation and Environment*, vol. 8, no. 3, pp. 125–129, 1994.

[18] J. Chen, Z. Zou, and X. Pang, "Digging performance characterization for hydraulic excavator considering uncertainty during digging operation," *Proceedings of the Institution of Mechanical Engineers, Part C: Journal of Mechanical Engineering Science*, vol. 232, no. 5, pp. 857–871, 2018.

[19] B. Zhang, S. Wang, Y. Liu, and H. Yang, "Research on trajectory planning and autodig of hydraulic excavator," *Mathematical Problems in Engineering*, vol. 2017, Article ID 7139858, 10 pages, 2017.

[20] X. Li, G. Wang, S. Miao, and X. Li, "Optimal design of a hydraulic excavator working device based on parallel particle swarm optimization," *Journal of the Brazilian Society of Mechanical Sciences and Engineering*, vol. 39, no. 10, pp. 3793–3805, 2017.